Applied Computer Science 2026, vol. 22, no. 1, pp. 199–213
https://doi.org/10.35784/acs_8034

Submitted: 2025-07-03 | Revised: 2025-09-07 | Accepted: 2025-09-24

Keywords: bone fracture severity, vibration analysis, frequency response function (FRF), non-destructive testing, biomechanical diagnostics

Jignesh JANI [1*], *Nikunj RACHCHH* [1]
[1] Marwadi University, India, jignesh.jani@marwadieducation.edu.in, nikunj.rachchh@marwadieducation.edu.in
[*] Corresponding author: jignesh.jani@marwadieducation.edu.in

Development of non-destructive vibration method for classification of bone fracture severity

Abstract

Accurate classification of bone fracture severity is critical in orthopedic evaluation. Radiation-based methods such as X-ray, CT, and MRI provide anatomical detail but lack the ability to classify fracture severity. This study presents a non-invasive, vibration-based approach to assessing fracture severity by analyzing dynamic response characteristics. Five goat (metacarpal) bone specimens were examined, including one unfractured bone that served as a reference bone and four with induced fractures in the lateral, longitudinal, and two oblique orientations. Controlled impact excitation was applied using an impact hammer, and acceleration responses were measured using acceleration sensors. Frequency response function (FRF), coherence, and phase shift were calculated using Fast Fourier Transform (FFT) algorithms. Resonance frequency and FRF magnitude served as primary indicators of stiffness loss and damping changes caused by fractures. The reference bone had a resonance frequency of 376 Hz and an FRF magnitude of 12.96 g/N, which was considered the reference parameter. The lateral fracture showed the most severe response, with a 17.98% increase in resonant frequency and a 491% increase in FRF magnitude, indicating significant stiffness redistribution and low damping. Longitudinal and oblique fractures resulted in large resonant frequency reductions of up to 94.4%. The experimental results were obtained using Fast Fourier Transform (FFT) algorithms and Euler-Bernoulli ray theory. These results suggest that vibration analysis is a reliable, quantitative, and non-destructive tool for classifying the severity of bone fractures.

1. INTRODUCTION

Bone fractures are among the most common musculoskeletal injuries with a significant impact on quality of life. The incidence of bone fractures is increasing worldwide due to an aging population, high-impact trauma, osteoporosis, and point injuries (Amin et al., 2014; Hoogervorst et al., 2020; Hui et al., 1988; Keen, 2003; Omsland et al., 2011; Wu et al., 2021). To accurately diagnose fractures and their severity, the gold standard radiation-based techniques such as X-rays, CT scans, and MRIs have been used in clinical trials (Healthline, n.d.). Research on non-invasive and vibration-based techniques for determining bone integrity began in the early 20th century (Lippmann, 1932) and has evolved with technological improvements in sensors and vibration signal processing (Ali, 2019; Jani & Rachchh, 2022; Karpiński, 2022; Karpiński et al., 2019; Leitgeb, 1986; Nikiforidis et al., 1990; Van der Perre et al., 1983; Van der Perre & Lowet, 1996). Vibration analysis provides characterized changes in mechanical properties such as stiffness, damping, and resonant natural frequency parameters that are directly affected by fractures. Current research on the vibrational behavior of fractured bone has grown exponentially (Karpiński et al., 2023; Machrowska et al., 2024; Wang et al., 2015; Zimmermann et al., 2015). A fracture introduces discontinuities that scatter wave propagation and can be identified by vibrational parameters such as frequency response function (FRF), coherence loss, and phase shifts (Kadhim et al., 2024). Fracture orientation plays an important role in identifying the severity of a fracture, which serves as a high mechanical impact on the bone (Behiri & Bonfield, 1989; Dong et al., 2012; Marco et al., 2018; Melvin, 1993). Consider common clinical fracture types (longitudinal, transverse, and oblique) (Kadhim et al., 2024; Sim et al., 2021) In this study, four fracture orientations were experimentally simulated: lateral (perpendicular to the bone axis), longitudinal (parallel to the axis), and 45° oblique (left-to-right and right-to-left). Each fracture orientation affects stiffness and vibration parameters differently (Bone

Fractures: Types, Symptoms & Treatment n.d.; Cohen et al., 2017; Ritchie et al., 2005; Yoon et al., 2021; Zimmermann et al., 2015).

X-rays, CT scans, and MRI provide a static representation of the fracture location on the bone, but this radiographic method fails to evaluate how the fracture affects reduction or increment of bone stiffness and structural damping. This non-invasive vibration based technique aims to develop a bridge between radiation techniques to identify fractures and reduction in bone stiffness and structural damping. The main objective of this experimental work is to classify fracture severity based on the orientation of the fracture.

2. MATERIAL AND METHODOLOGY

2.1. Bone specimens

2.1.1. Sample selection and ethical approval

In this study, goat(metacarpal)bones were obtained from slaughterhouses in Rajkot, Gujarat, India. The study protocol was approved by the institutional ethics committee of Marwadi University. Soft tissues were removed from the bones using formaldehyde solution and then air dried to ensure uniform preparation and ease of handling during vibration testing.

2.1.2. Specimen description and fracture modeling

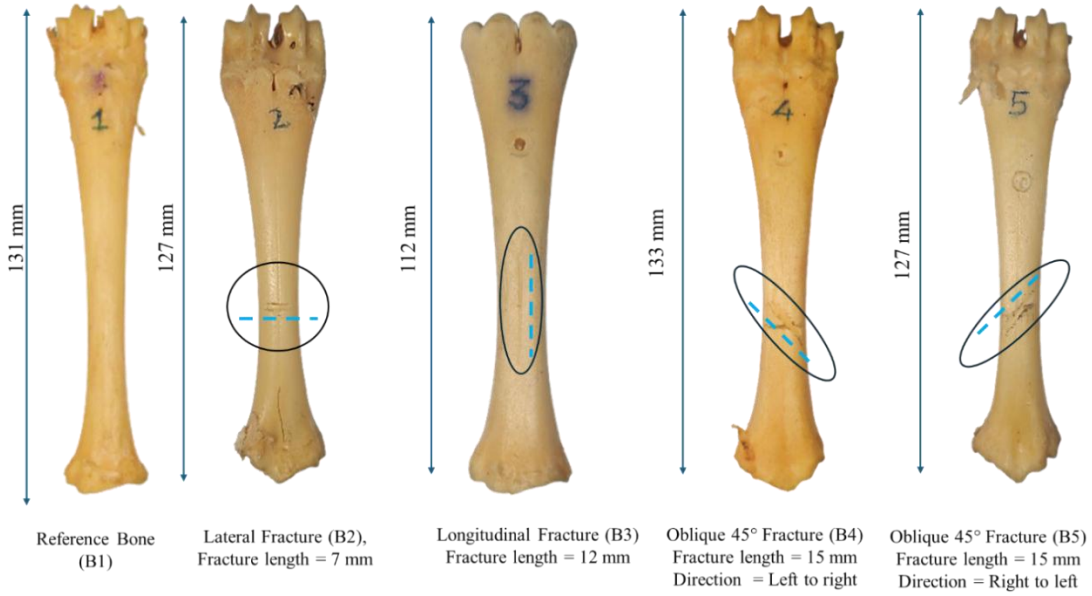

Fig. 1. Bone specimens with varying fracture orientations

Figure 1 describes five bone specimens (B1 through B5), each a bone with a specific fracture orientation, size, and bone length used for vibration-based structural integrity assessment. Table 1 provides meaningful bone and fracture parameters for experimental work.

Tab. 1. Bone specimen fracture geometry and parameters

Specimen ID	Fracture Orientation	Fracture Length (mm)	Bone Length (mm)
B1	None (Reference)	0	131
B2	Lateral (⊥ to bone axis)	7	127
B3	Longitudinal (∥ to bone axis)	12	112
B4	45°Oblique fracture (Left to Right)	15	133
B5	45°Oblique fracture (Right to Left)	15	127

2.2. Experimental hardware setup

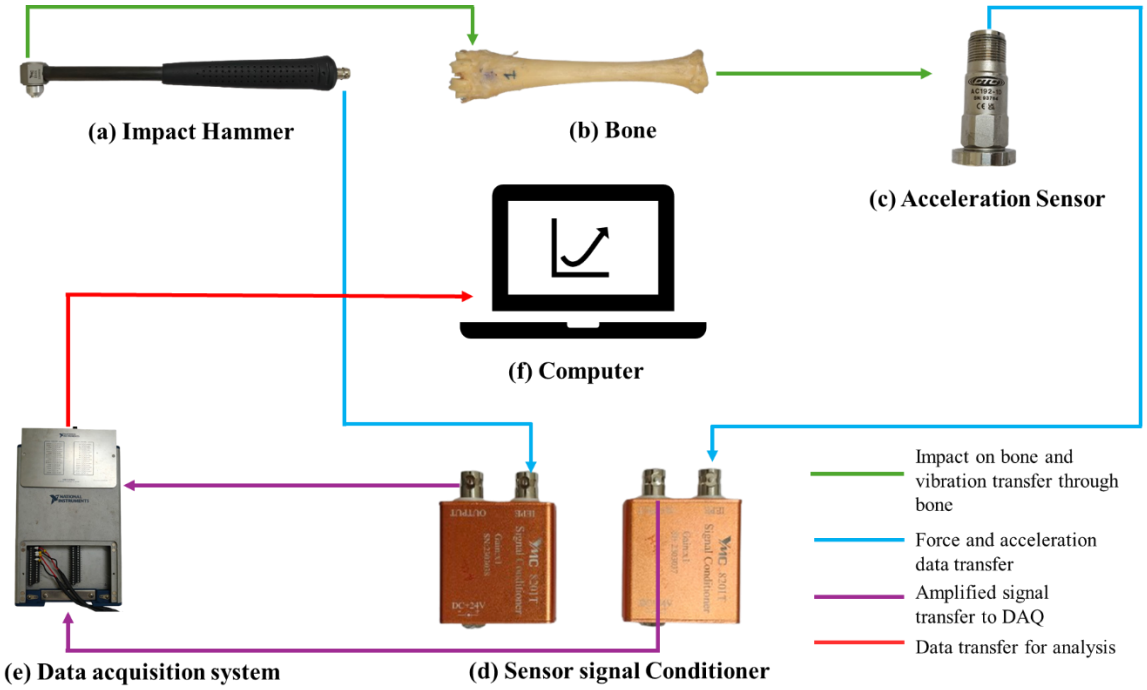

Fig. 2. (a) Impact hammer (YMC – IH-01); (b) Bone; (c) Acceleration sensor (CTC -AC192-1D); (d) Sensor signal conditioner; (e) Data acquisition system (NI – USB 6341); (f) Computer with sigview software

The Impact Hammer (Fig. 2a) provides external excitation of bone specimens with controlled force pulses. This impact hammer is equipped with a built-in force sensor with a sensitivity of 2.25 mV/N. The bone specimen (Fig. 2b) is mounted with an acceleration sensor (Fig. 2c) to record the acceleration response. Accelerometers have a sensitivity of 100 mV/g and a frequency range of 1 Hz to 10 kHz. The acceleration sensor provides real-time vibration signals to the data acquisition system through a signal conditioner, which is then processed by Sigview software. A sensor signal conditioner (Fig. 2d) is used to amplify force and acceleration signals, reduce unwanted noise, and stabilize dynamic measurements. Data Acquisition System (Figure 2e), which collects real-time data from the signal conditioner and acts as a bridge between the sensor and the software interface. The data acquisition system is capable of acquiring analog inputs with 16-bit resolution, 500 kS/s sampling rate, and ±10 V input range, providing accurate signal acquisition, which is critical for vibration analysis. A computer running Sigview software (Fig. 2f) analyzed the real-time data received from the data acquisition system.

2.3. Experiment methodology

Each bone specimen was properly clamped in a mechanical vice with one end free for impact application. The impact hammer was used to carefully apply a longitudinal impact to the free end of the bone, as shown in Figure 3. An acceleration sensor was mounted near the clamped end of the bone to measure the vibrational response along the longitudinal axis of the bone. The input force and corresponding output acceleration signals were acquired by a data acquisition (DAQ) system and monitored in real time by Sigview software. The acquired signals were analyzed by calculating the frequency response function (FRF), coherence function, and phase shift characteristics using built-in Fast Fourier Transform (FFT) algorithms within the software. Each test was performed three times per specimen and the results averaged to ensure experimental repeatability and manual influence differences (Ewins, 2009).

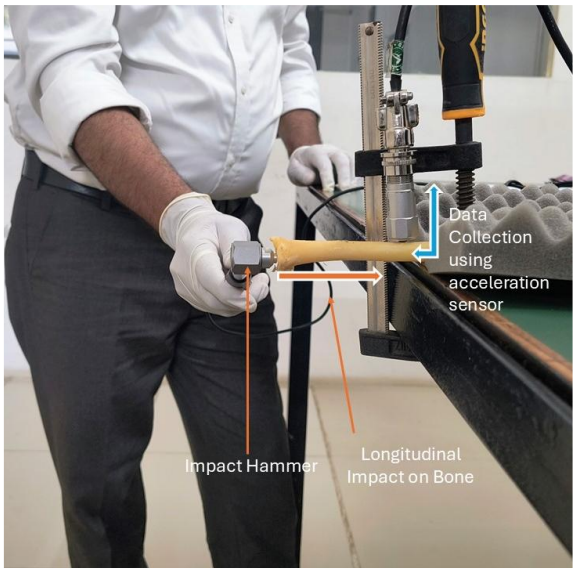

Fig. 3. Experimental setup for longitudinal impact testing on bone for vibration analysis

2.4. Data processing

The vibrational response of bone is influenced by both the direction of impact and the orientation of the fracture. To study such behavior, three essential vibration parameters must be considered: resonant natural frequency, coherence function, and phase shift response. The frequency response function (FRF) is a very common method for studying the dynamic characteristics of solid objects (Pinzaru et al., 2024; Siemens, n.d.). FRF converts a time-domain signal to a frequency-domain signal using a transfer function that connects the input (from the hammer) and the output (from the accelerometer) (Kadhim et al., 2024). By interpreting the FRF, it is possible to derive the resonant natural frequency, damping characteristics and mode shape. The vibration response of the solid object is divided into three parts: Stiffness controlled zone at a frequency lower than the resonant natural frequency, Damping controlled zone at the resonant natural frequency and Mass controlled zone at a higher frequency above the resonant natural frequency. Coherence function validates a measure of the FRF, how well the two signals (input and output) are correlated at each frequency, ranging from 0 (no correlation) to 1 (perfect correlation) (Allemang et al., 2022; SDynPy, n.d.).

2.5. Parameter estimation

Bone integrity assessment involves the calculation of parameters from vibration signals. The natural resonant frequency of the bone is identified from the maximum peak observed in the frequency response function (FRF) plot. The stiffness ratio is calculated from the resonant eigenfrequency of the fractured bone relative to the bone, which helps to identify loss of structural integrity. The coherence value is associated with the linear relationship between the applied input force and the measured acceleration response. A coherence value close to 1 indicates minimal energy loss and reliable vibration signal transmission through bone. Another verification parameter to consider is phase shift analysis. It can focus specifically on delays and distortions in the structural response resulting from energy absorption at fracture sites. This approach allows all parameters to be continuously monitored across all bone specimens, providing a direct comparative assessment of the severity of fracture orientation in bone. To support the experimental resonance natural frequency results, the bone was assumed to behave like a slender cantilever beam, and analytical natural frequency estimates using Euler-Bernoulli theory were used to validate the observed trends.

3. THEORETICAL BACKGROUND

The theoretical background for the analysis of vibrational behavior required a combination of vibration theory and fracture mechanics to explain how bone responds to dynamic loading. Euler-Bernoulli beam theory evaluates natural frequency shifts due to changes in stiffness caused by fracture. Linear Elastic Fracture Mechanics (LEFM) describes how stress concentration at crack tips leads to structural failure.

3.1. Vibrational approach in bone

To understand the vibrational behavior of fractured bone, the resonant frequency (f_n)of a structure such as a cantilever beam can be estimated using the Euler-Bernoulli beam theory. During the experiment, the slender bone specimens are assumed to behave like cantilever beams. The natural frequency is expressed as:

$$f_n = \frac{\beta_n^2}{2\pi}\sqrt{\frac{EI}{\rho AL^4}} \tag{1}$$

where f_n is the natural frequency in Hz, β_n is the mode shape coefficient, E is Young's modulus representing bone elasticity, I is the area moment of inertia of cross section, ρ is the density of the bone, A is the cross sectional area, and L is the length of the bone. This equation clarify that the natural frequency is directly proportional to the square root of the flexural stiffness (EI) and inversely proportional to the square root of the bone length. So, any changes in stiffness or in geometry due to fractures will cause important changes in the vibration signature. This theoretical foundation is a key method in interpreting the shifts in resonance frequency and variations in damping observed experimentally (Bishop, 1955; Chondros et al., 2001; Dimarogonas, 1996)

3.2. Fracture mechanics approach in bone

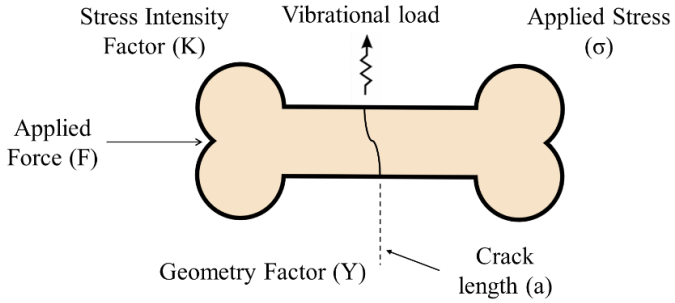

Fig. 4. Schematic of cracked bone showing applied stress (σ), Crack length (a), Geometry factor (Y), Stress intensity factor (K), and energy release rate under vibrational loading

Figure 4 shows how a bone with a crack behaves under stress, which can be explained by linear elastic fracture mechanics (LEFM), which quantifies the strength of the stress concentration near the crack tips (Behiri & Bonfield, 1989; Ritchie et al., 2005). This theory helps us understand how stress builds up at the tip of a crack. Stress intensity factor (K) is calculated as:

$$K = Y\sigma\sqrt{\pi a} \tag{2}$$

where K is the stress intensity factor, σ is the applied force, $a$is the length of the crack and Y *is* a shape factor based on the bone and crack geometry. When K becomes greater than a critical limit K_{IC} the crack can grow rapidly and cause the bone to fracture (Behiri & Bonfield, 1989; Melvin 1993). Another related value is the energy release rate (G), which tells us how much energy it takes for a crack to grow. It is related to K by the equation.

$$G = \frac{K^2}{E'} \tag{3}$$

where $E'$is the adjusted stiffness of the bone, which depends on whether the bone is under simple plane stress conditions (Zimmermann et al., 2015). These equations help explain how cracks affect bone strength and how vibration can reveal hidden damage by analyzing energy loss and stiffness reduction (Ritchie et al., 2005).

4. RESULTS

4.1. Reference bone: Case -1

Fig. 5 shows the results of vibration tests on the reference bone (B1), which provide dynamic characteristics to identify the natural frequency using the frequency response function (FRF), which gives a resonant natural frequency of 376 Hz and a FRF magnitude of 12.96 g/N (Fig. 5a). This value serves as a baseline for comparison with the fractured bone case. The resonant natural frequency occurs in the damping control zone (shaded orange), which reflects effective energy transfer as well as normal damping characteristics. Because the damping zone is narrow, it indicates high stiffness in the reference bone. In the low frequency range (stiffness control zone shaded green), the response at a low FRF magnitude would be less than 12.26 g/N, indicating that the bone is structurally stiff and intact. This identity reference bone remains stiff and behaves normally when force is applied. The phase plot (Figure 5b) shows a sudden drop to approximately -170° at the resonant natural frequency. The sudden phase shift indicates resonance at the resonant natural frequency (376 Hz) and verifies that the system is making the normal transition from stiffness-dominated to mass-dominated behavior. To further verify the resonant natural frequency, the coherence function (Figure 5c) for the reference bone does not remain close to 1.0 in the frequency range of 350 Hz to 390 Hz. A coherence value close to 1 provides a linear relationship between the input (impact force) and the output (acceleration response). This coherence measures the signal, which provides reliability, and the system response is consistent and repeatable, with minimal noise or non-linear effects.

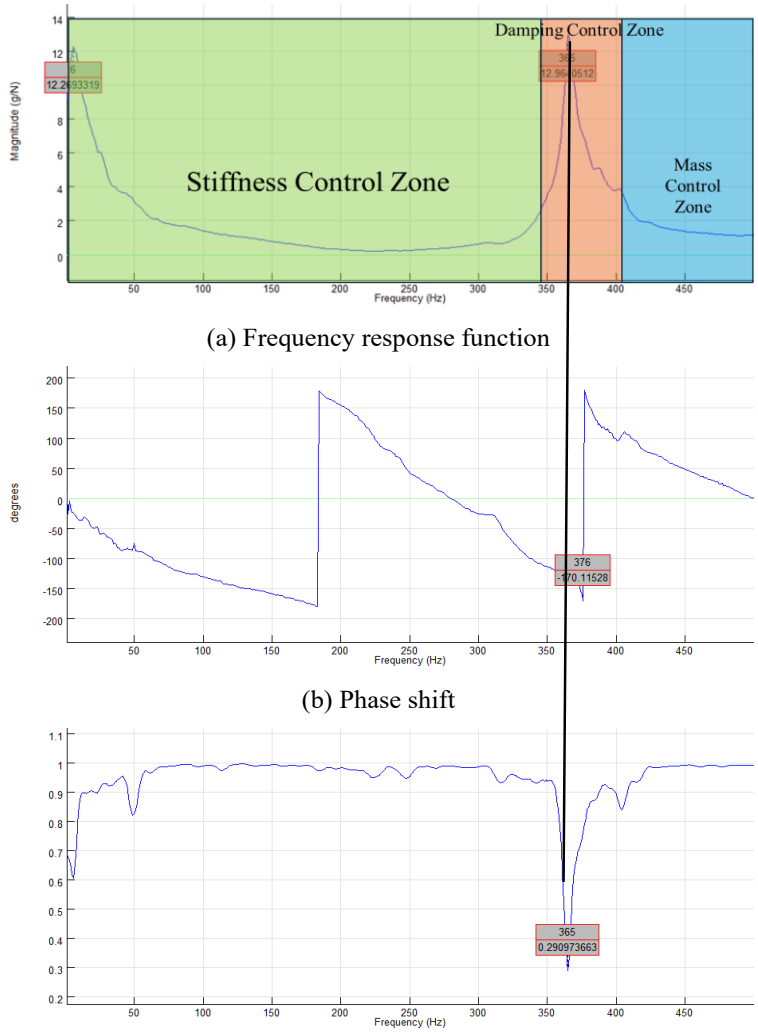

Fig. 5. Vibration response of reference bone (B1): (a) FRF showing resonance peak at 376 Hz; (b) phase shift confirming resonance; (c) coherence validating signal reliability

4.2. Lateral fracture bone: Case – 2

Fig. 6 shows the results of the vibration response of the bone with a lateral fracture found by its frequency response function (FRF), phase angle, and coherence function plots. In the FRF plot (Fig. 6a), a resonant natural frequency peak is observed at 444 Hz, with an unexpectedly high FRF amplitude of 76.49 g/N. This resonant eigenfrequency shifts beyond 400 Hz and shrinks the damping zone (shaded orange) with a high FRF magnitude of 76.49 g/N , which is a clear indication of the low damping found in the bone due to the lateral fracture and the local stiffness redistribution increase around the fractured area. Compared to a reference bone, there is a severe reduction in structural stiffness and energy absorption capability due to the lateral fracture. This pattern shows a clear, wide range of stiffness control zone (shaded green) and shrinking damping zone. A fracture in the bone has compromised its ability to resist deformation. The corresponding phase shift plot (Fig. 6b) shows a rapid phase shift occurring around the same frequency, with the phase reaching approximately 150° at 444 Hz. This sharp change establishes the presence of resonance at 444 Hz, and the output acceleration of the bone becomes out of phase with the input force. Such a sharp change in the phase response is caused by the fracture-induced discontinuity. In addition, the coherence function plot (Fig. 6c) shows a significant decrease in the coherence value to 0.4869 at the resonance frequency. In general, coherence values close to 1, indicating reliable input force and output acceleration, have a linear relationship. At 444 Hz, the decrease in coherence observed here suggests the presence of nonlinear behavior at the resonant frequency of 444 Hz, likely due to nonlinearity at the resonant natural frequency due to the presence of fractures in the bone.

(a) Frequency response function

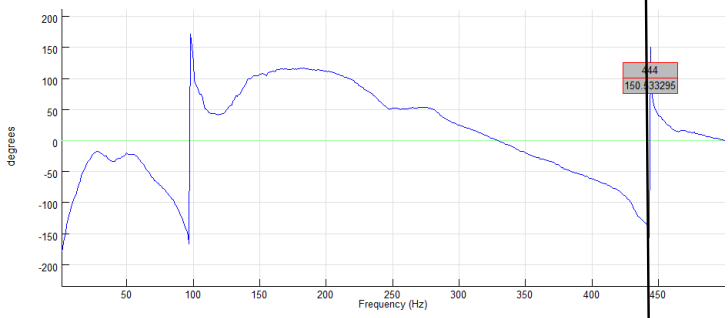

(b) Phase shift

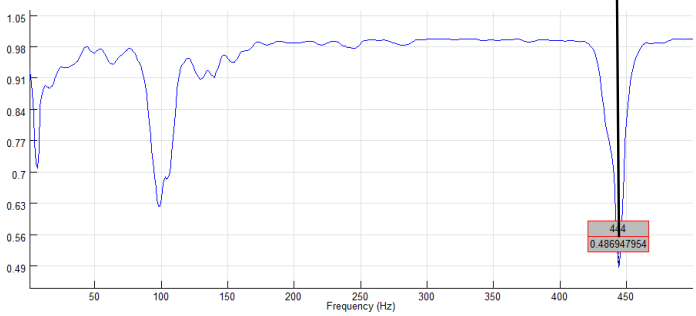

(C) Coherence

Fig. 6. Vibration response of lateral fracture bone (B2): (a) FRF showing resonance peak at 444 Hz; (b) phase shift confirming resonance; (c) coherence validating signal reliability

4.3. Longitudinal fracture bone: Case – 3

Figure 7 shows the results of the vibrational response of the bone with a longitudinal fracture found through its frequency response function (FRF), phase angle, and coherence function plots. In the FRF plot (Fig. 7a), a resonant natural frequency peak is observed at 102 Hz with an FRF magnitude of 10.82 g/N. This resonant eigenfrequency, located below the damping zone (shaded orange), shifted toward the stiffness control zone (shaded green) and the stiffness control zone shrank. Compared to the reference bone, the shift of the damping zone establishes a significant reduction in structural stiffness due to longitudinal fracture. The phase shift (Fig. 7b) supports this finding, showing a sharp phase shift change near the resonant natural frequency. At 102 Hz, the phase angle drops to approximately -171.8°, a typical indication of resonance. This abrupt change in phase reflects the point at which the bone structure no longer moves in synchrony with the applied force, further establishing the influence of the fracture on its dynamic response. The coherence function plot (Fig. 7c) shows a minimum of 0.711 at approximately 102 Hz, indicating a moderate decrease in coherence. However, the coherence is consistently close to 1 over a wide range of frequencies.

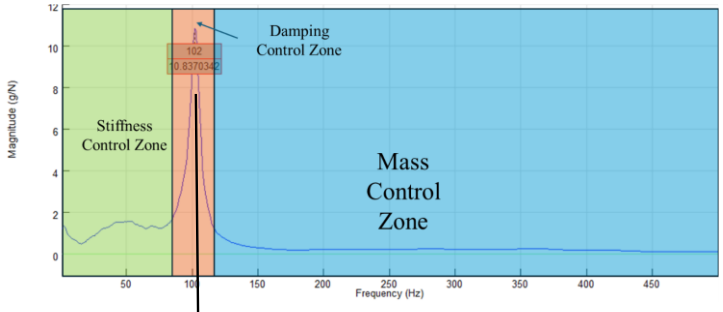

(a) Frequency response function

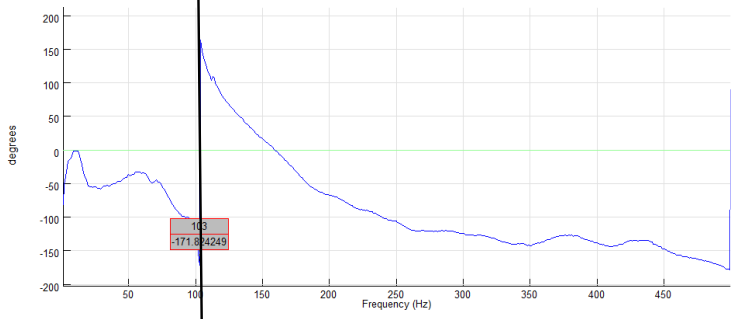

(b) Phase shift

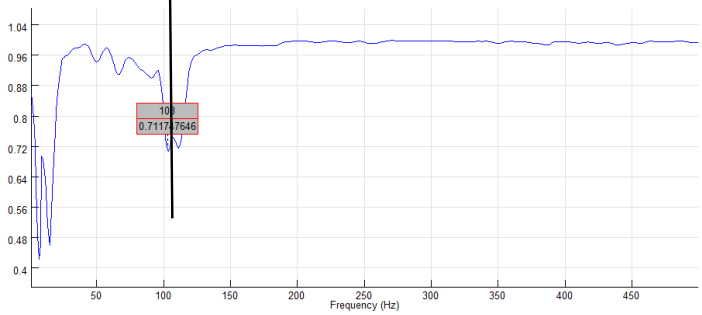

(C) Coherence

Fig. 7. Vibration response of longitudinal fracture bone (B3): (a) FRF showing resonance peak at 102 Hz, (b) phase shift confirming resonance, (c) coherence validating signal reliability

4.4. Oblique fracture bone (45° Left to right): Case – 4

Figure 8 shows the results of the vibration response of the oblique fracture bone (45° left to right). The frequency response function (FRF) (Fig. 8a) shows the reduced resonance natural frequency is 21 Hz and shifted to the lower end of the graph, which shrinks more of the stiffness control zone (shaded green), while

the FRF magnitude is found to be 17.68 g/N, indicating a higher damping effect compared to the reference bone. The phase shift graph (Fig. 8b) shows changes in the resonant natural frequency at 21 Hz, recorded at -30°, which is relatively flat and lacks the typical steep drop seen in moderately fractured bones. The coherence plot (Fig. 8c) shows a dip at the same resonant natural frequency of 21 Hz, and its coherence value is 0.192. This coherence value indicates low correlation between the input and output signals, often caused by nonlinearities and energy scattering introduced by the fracture on the bone surface. Such low coherence at the resonant frequency is a strong indication that the oblique fracture has perturbed the vibrational integrity of the bone.

4.5. Oblique fracture bone (45° Right to left): Case – 5

Figure 9 shows the results of the vibration response of an oblique fracture bone (45° right to left). The primary resonant eigenfrequency in the frequency response function (FRF) plot (Fig. 9a) is significantly reduced to 22 Hz, which moves to the lower part of the spectrum. This process creates a smaller stiffness control zone (shaded green). Its corresponding FRF magnitude is 24.40 g/N, which is the highest of all fracture cases and represents excessive stiffness loss. There is a second but smaller peak at 398 Hz with a FRF magnitude of 2.31 g/N. This low and broad peak indicates the presence of a highly damped second mode shape. The phase plot (Fig. 9b) also shows two prominent transitions. The first is at a frequency of about 22 Hz with a phase angle of +30°, which is anomalous with respect to the abrupt negative dip present in healthy bone. The second transition is at a frequency of about 398 Hz with a phase angle of +2.84°, representing a more fragile segment that may be susceptible to failure at high frequencies due to intense damping effects. The coherence plot (Fig. 9c) confirms these results. Two significant dips in coherence are found: at 22 Hz with a value of 0.0217 and at 398 Hz with a value of 0.1194. These low values indicate reduced signal reliability and confirm the resonant behavior at both frequencies.

5. DISCUSSION

Figure 10 includes all the frequency response functions (FRFs) of the bone specimens (B1 through B5) and shows how fractured bone responds dynamically at different frequencies. The reference bone (B1), representing a reference bone (unfractured bone), has a clear resonance natural frequency peak at 376 Hz with a moderate FRF magnitude of 12.96 g/N. This response is used as reference data for a comparative study of other fractured cases. Once a fracture was introduced into the bone, the vibration pattern of the fractured bone changed dramatically. The lateral fracture bone (B2) shows a resonant natural frequency peak at 444 Hz, significantly higher than the reference bone, with the highest FRF magnitude of 76.49 g/N. This measurement indicates a severe loss of damping and likely stiffness redistribution around the fracture zone; the response peak is also very narrow and sharp, compared to the fractured bone peak. A sharp peak is indicative of low damping and a narrow curve is indicative of concentrated stiffness, reflecting the fracture-induced discontinuity.

In contrast, the longitudinal fracture (B3) shows a significant reduction in resonance frequency to 102 Hz, indicating a loss of axial stiffness. The corresponding FRF value of 10.83 g/N indicates that the bone has become more flexible due to the fracture being parallel to the bone axis. Some surprising effects were found in the oblique fractures. The left-to-right oblique fracture bone (B4) found a resonance peak natural frequency at 21 Hz with a moderate FRF magnitude of 17.68 g/N, representing a reduction in both stiffness and structural integrity. The right-to-left oblique fracture bone (B5) exhibited dual mode behavior with resonance peaks at 22 Hz and 398 Hz. The first peak (24.40 g/N) indicates a strong low-frequency response, while the second peak indicates that the fractured segment vibrates independently at a higher mode. This split response is a strong indication of localized flexibility and mode shape distortion, likely due to fracture propagation and asymmetric geometry.

The pronounced decrease in resonant frequency observed for oblique fractures (B4 and B5) can be attributed to their effect on bending stiffness and load distribution. Unlike longitudinal fractures, which mainly reduce axial stiffness, oblique fractures simultaneously compromise axial and lateral load transfer, creating highly unstable mechanical conditions. This results in drastic frequency reductions to the 21-22 Hz range.

Clinically, oblique fractures are considered unstable because the shear forces along the oblique fracture plane promote displacement and often require surgical fixation for stabilization. These findings are consistent with the clinical understanding of fracture biomechanics and highlight the diagnostic potential of vibration-

based methods. In addition, our results complement previous studies using vibration-based bone diagnostics, such as demonstrated vibration screening in long bones (Ali, 2019). Transverse vibration for fracture diagnosis and analyzed the effect of boundary conditions on fracture bone dynamics (Yoon et al., 2021; Sim et al., 2021). Taken together, these works reinforce the role of vibration analysis as a promising non-invasive tool for biomechanical and orthopedic applications.

Goat metacarpals provide a simple experimental model because they are readily available and have structural similarities to human bones (Fan et al., 2014). However, there are notable differences with respect to human bone such as geometry, density, and microstructure. Similar vibration-based experiments have also been performed on human cadaver bone (Sim et al., 2021; Yoon et al., 2021). These studies, along with the work presented here, demonstrate the feasibility of vibration-based diagnostics as a basis for future applications in human bone fracture detection and healing assessment (Doemland et al., 1986; Mattei et al., 2018).

This research is limited by the small sample size of five representative bones, which limits the statistical power and validity of the results. However, the experimental results provide a clear proof of concept for vibration-based bone fracture severity classification. In future work, the study will be extended to a larger set of specimens, including human cadaveric bones and specimens with variations in gender and weight, to improve statistical reliability and clinical application.

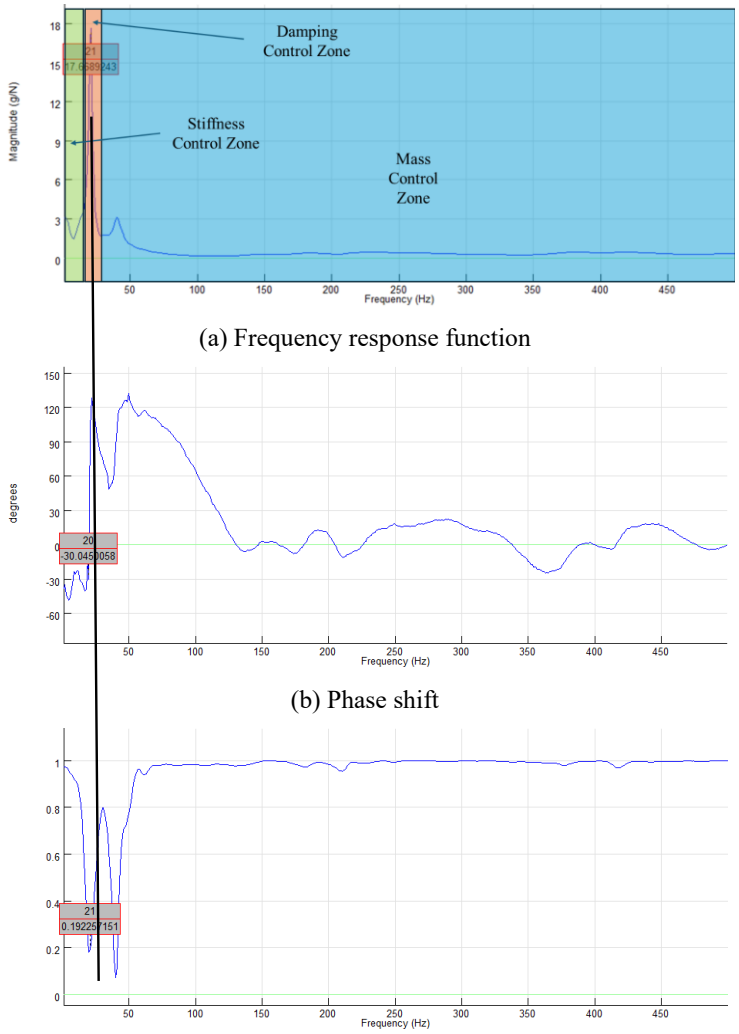

Fig. 8. Vibration response of oblique fracture (45° left to right) bone (B4) : (a) FRF showing resonance peak at 21 Hz (b) phase shift confirming resonance (c) coherence validating signal reliability

For future clinical use, the method can be adapted to in vivo conditions. Unlike excised bone testing, in vivo fracture testing is subject to surrounding soft tissues and joint constraints that introduce additional damping and noise into the vibration response. To address this, non-invasive excitation methods such as low-energy impactors or ultrasound pulses will be used in conjunction with miniaturized wearable accelerometers to safely record signals. Advanced signal processing techniques will also be critical to eliminate biological noise and extract bone-specific vibration features. These developments, supported by previous cadaveric and human-focused studies (Ali, 2019; Sim et al., 2021; Yoon et al., 2021)), highlight the translational value of the method, while acknowledging that further validation is required before clinical application.

Overall, the key findings are summarized in Table 2 and Figure 11, which highlight how fracture orientation has a direct and measurable effect on resonant natural frequency, amplitude, and mode behavior. These findings support the use of vibration analysis as a reliable, non-destructive method for evaluating fracture severity and structural degradation in bone.

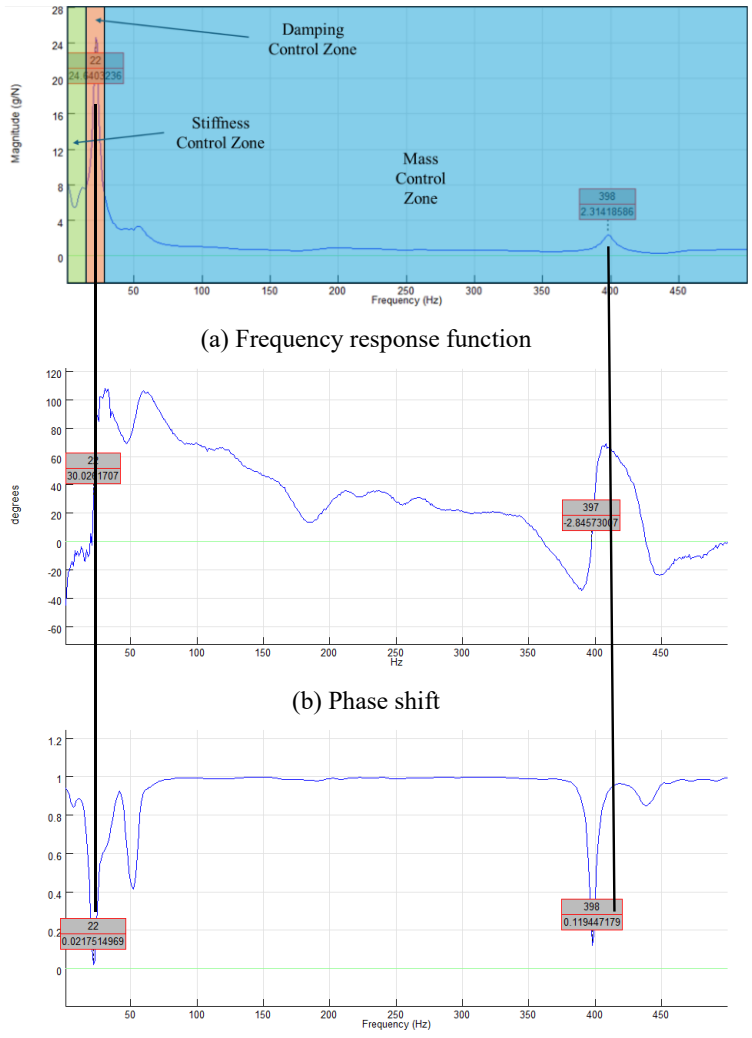

(a) Frequency response function

(b) Phase shift

(C) Coherence

Fig.9. Vibration response of oblique fracture (45° right to left) bone (B5): (a) FRF showing resonance peak at 22 Hz, (b) phase shift confirming resonance, and (c) coherence validating signal reliability

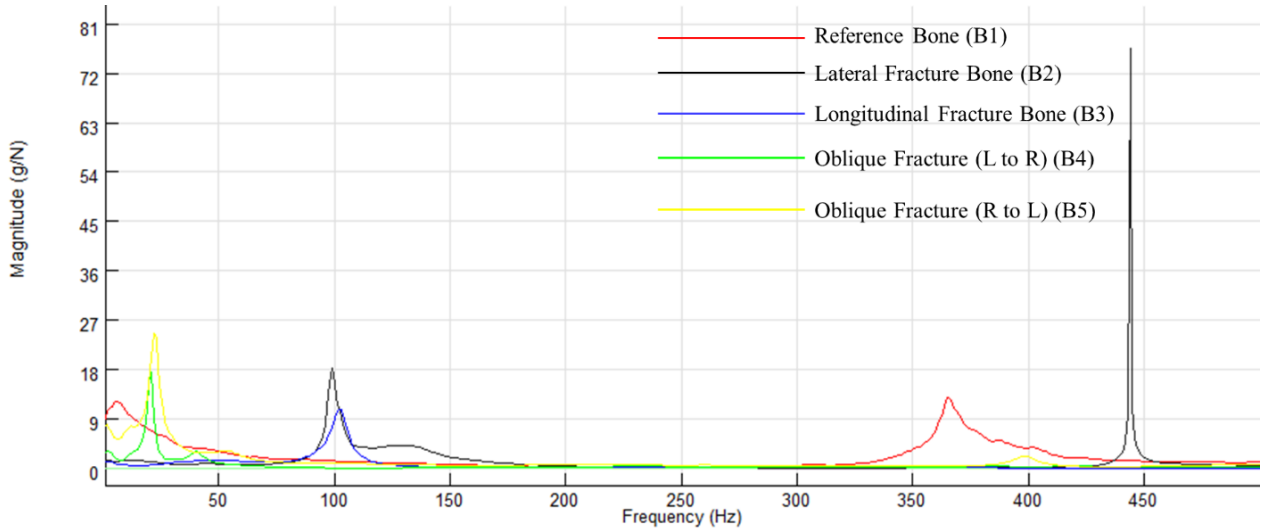

Fig 10. Comparative study on experimental result of frequency response function for all bone (B1 to B5)

Tab. 2. Result summary of experimental bone dynamic parameters

Specimen ID	Fracture Type	Resonance Frequency (Hz)	FRF Magnitude (g/N)	Coherence Value	Severity level*
B1	Reference (No fracture)	376	12.96	0.29	No issue due to no fracture
B2	Lateral	444	76.49	0.4869	Very high
B3	Longitudinal	102	10.83	0.711	Low
B4	Oblique (45° L to R)	21	17.68	0.192	Moderate
B5	Oblique (45° R to L)	22	24.4	0.0217	Moderate

*Severity level is classified based on reduction in resonance frequency, increase in FRF magnitude, and decrease in coherence value compared to the reference bone.

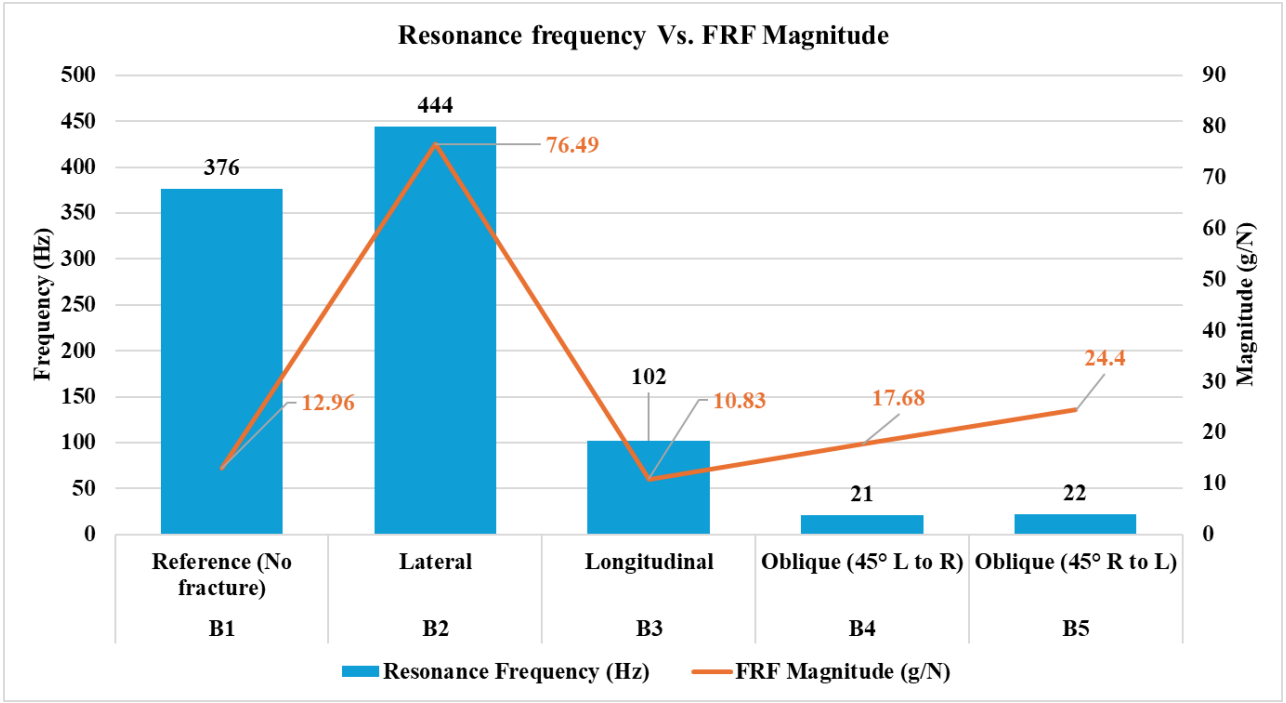

Fig. 11. Resonance frequencies and peak magnitudes of the Frequency Response Function (FRF) for bone specimens with differing fracture orientations, demonstrating changes in stiffness and damping as a result of fracture severity

6. CONCLUSIONS

The experimental results showed that different orientations of fractures result in unique vibration patterns that clearly identify and classify fracture severity. The reference bone (B1) showed dynamic characteristics with a resonance frequency of 376 Hz. The phase shift and coherence plots also confirm the same. When all the fracture cases are compared with the reference bone (B1), the lateral fracture bone (B2) shows a 17.98% increase in resonance frequency from 376 Hz to 444 Hz and a 491% increase in FRF magnitude from 12.96 g/N to 76.49 g/N, which is the most severe fracture state among all the cases due to the pronounced stiffness loss and low damping. The longitudinal fracture (B3) decreases 72.87% in resonance natural frequency from 376 Hz to 102 Hz and decreases 16.45% in FRF magnitude from 12.96 g/N to 10.83 g/N, confirming it as the least severe case with minor structural degradation. The oblique fracture bone (B4) decreases 94.4% in resonance natural frequency from 376 Hz to 21 Hz and increases 36.3% in FRF magnitude from 12.96 g/N to 17.68 g/N, indicating moderate severity. Similarly, the oblique fracture (B5) had a 94.1% decrease in resonance frequency from 376 Hz to 22 Hz and an 88.3% increase in FRF magnitude from 12.96 g/N to 24.4 g/N, also in the moderate severity category.

Overall, the results show that lateral cracks have the most critical stiffness loss, while longitudinal and oblique cracks have less, but still moderate, effects. The study supports the use of the vibration-based method as a non-invasive and measurable method to evaluate fracture severity in bone, providing valuable insights for orthopedic diagnostics and future biomechanical research. The proposed vibration-based approach can be used as a supportive diagnostic tool in orthopedics, complementing radiographic imaging by allowing non-invasive classification of fracture severity and monitoring of healing progress.

Funding

This research was funded by NewGen IEDC, Government of Gujarat, India in collaboration with Marwadi University, Rajkot, Gujarat, India. Approval ID: ECR/356/Indt/GJ/2022.

Conflicts of Interest

The authors have no relevant financial or non-financial interest to disclose.

Availability of Data and Material

All the data that support the findings of this study are incorporated in the manuscript.

Ethical Approval

This study was approved by Marwadi University Ethics Committee (ECR/356/Indt/GJ2022).

Acknowledgments

In order to convey their heartfelt appreciation to the NewGen IEDC, Government of Gujarat, for giving financial assistance to this project, the authors would like to express their own genuine thanks. In addition, we would like to express our deepest gratitude to Marwadi University for providing us with an outstanding academic platform as well as the essential infrastructure and resources that made it possible for us to effectively carry out the experimental work.

REFERENCES

Ali, R. (2019). *Bone vibration analysis as a novel screening tool for long bone fractures*. Doctoral, Sheffield Hallam University.

Allemang, R. J., Patwardhan, R. S., Kolluri, M. M., & Phillips, A. W. (2022). Frequency response function estimation techniques and the corresponding coherence functions: A review and update. *Mechanical Systems and Signal Processing*, *162*, Article 108100. https://doi.org/10.1016/j.ymssp.2021.108100

Amin, S., Achenbach, S. J., Atkinson, E. J., Khosla, S., & Melton, L. J. (2014). Trends in fracture incidence: A population-based study over 20 years. *Journal of Bone and Mineral Research*, *29*(3), 581–589. https://doi.org/10.1002/jbmr.2072

Behiri, J. C., & Bonfield, W. (1989). Orientation dependence of the fracture mechanics of cortical bone. *Journal of Biomechanics*, *22*(8–9), 863–872. https://doi.org/10.1016/0021-9290(89)90070-5

Bishop, R. E. D. (1955). Vibration problems in engineering (Third Edition). S. P. Timoshenko (with the collaboration of D. H. Young). D. Van Nostrand, New York, 1955. 468 Pp. Diagrams. 65s. *The Aeronautical Journal*, *59*(539), 781. https://doi.org/10.1017/S0368393100117183

Chondros, T. G., Dimarogonas, A. D., & Yao, J. (2001). Vibration of a beam with a breathing crack. *Journal of Sound and Vibration*, *239*(1), 57–67. https://doi.org/10.1006/jsvi.2000.3156

Cleveland Clinic. (n.d.). *Bone fractures: Types, symptoms & treatment*. Retrieved February 21, 2025, from https://my.clevelandclinic.org/health/diseases/15241-bone-fractures

Cohen, H., Kugel, C., May, H., Medlej, B., Stein, D., Slon, V., Brosh, T., & Hershkovitz, I. (2017). The influence of impact direction and axial loading on the bone fracture pattern. *Forensic Science International*, *277*, 197–206. https://doi.org/10.1016/j.forsciint.2017.05.015

Dimarogonas, A. D. (1996). Vibration of cracked structures: A state of the art review. *Engineering Fracture Mechanics*, *55*(5), 831–857. https://doi.org/10.1016/0013-7944(94)00175-8

Doemland, H. H., Jacobs, R. R., Spence, J., & Roberts, F. G. (1986). Assessment of fracture healing by spectral analysis. *Journal of Medical Engineering and Technology*, *10*(4), 180–187. https://doi.org/10.3109/03091908609022906

Dong, X. N., Acuna, R. L., Luo, Q., & Wang, X. (2012). Orientation dependence of progressive post-yield behavior of human cortical bone in compression. *Journal of Biomechanics*, *45*(16), 2829–2834. https://doi.org/10.1016/j.jbiomech.2012.08.034

Ewins, D. J. (2009). *Modal testing: Theory, practice and application* (2nd ed.). Wiley.

Fan, X., Ren, H., Chen, S., Wang, G., Deng, T., Chen, X., & Yan, Y. (2014). Comparative studies on the material performances of natural bone-like apatite from different bone sources. *Sheng wu yi xue gong cheng xue za zhi = Journal of Biomedical Engineering*, *31*(2), 352–356. https://europepmc.org/article/med/25039141

Healthline. (n.d.). *MRI vs. X-ray: Pros, cons, costs & more*. Retrieved April 9, 2025, from https://www.healthline.com/health/mri-vs-xray

Hoogervorst, P., Shearer, D. W., & Miclau, T. (2020). The burden of high-energy musculoskeletal trauma in high-income countries. *World Journal of Surgery*, *44*(4), 1033–1038. https://doi.org/10.1007/s00268-018-4742-3

Hui, S. L., Slemenda, C. W., & Johnston, C. C. (1988). Age and bone mass as predictors of fracture in a prospective study. *Journal of Clinical Investigation*, *81*(6), 1804–1809. https://doi.org/10.1172/JCI113523

Jani, J., & Rachchh, N. (2022). A journey from vibration measurements to machine learning base condition health monitoring: A brief review. In M. M. Noor, H. A. Tuan, & P. C. Mishra (Eds.), *Advances in mechanical and industrial engineering* (pp. 17–24). CRC Press.

Kadhim, A. J., Aubad, M. J., & Al-Juboori, A. M. (2024). Analyzing frequency response analysis experimentally for bone healing detection: Examining the potential of vibrational evaluations. *Diagnostyka*, *25*(3), 1–11. https://doi.org/10.29354/diag/192180

Karpiński, R. (2022). Knee joint osteoarthritis diagnosis based on selected acoustic signal discriminants using machine learning. *Applied Computer Science*, *18*(2), 71–85. https://doi.org/10.35784/acs-2022-14

Karpiński, R., Krakowski, P., Jonak, J., Machrowska, A., & Maciejewski, M. (2023). Comparison of selected classification methods based on machine learning as a diagnostic tool for knee joint cartilage damage based on generated vibroacoustic processes. *Applied Computer Science*, *19*(4), 136–150. https://doi.org/10.35784/acs-2023-40

Karpiński, R., Machrowska, A., & Maciejewski, M. (2019). Application of acoustic signal processing methods in detecting differences between open and closed kinematic chain movement for the knee joint. *Applied Computer Science*, *15*(1), 36–48. https://doi.org/10.23743/acs-2019-03

Keen, R. W. (2003). Burden of osteoporosis and fractures. *Current Osteoporosis Reports*, *1*(2), 66–70. https://doi.org/10.1007/s11914-003-0011-x

Leitgeb, N. (1986). A new noninvasive quantitative method for fracture diagnosis. *Medical Progress Through Technology*, *11*(4), 185–190. http://europepmc.org/abstract/MED/3543631

Lippmann, R. K. (1932). The use of auscultatory percussion for the examination of fractures. *The Journal of Bone & Joint Surgery*, *14*(1). https://journals.lww.com/jbjsjournal/fulltext/1932/14010/the_use_of_auscultatory_percussion_for_the.13.aspx

Machrowska, A., Karpiński, R., Maciejewski, M., Jonak, J., & Krakowski, P. (2024). Application of EEMD-DFA algorithms and ANN classification for detection of knee osteoarthritis using vibroarthrography. *Applied Computer Science*, *20*(2), 90–108. https://doi.org/10.35784/acs-2024-18

Marco, M., Belda, R., Miguélez, M. H., & Giner, E. (2018). A heterogeneous orientation criterion for crack modelling in cortical bone using a phantom-node approach. *Finite Elements in Analysis and Design*, *146*, 107–117. https://doi.org/10.1016/j.finel.2018.04.009

Mattei, L., Di Puccio, F., & Marchetti, S. (2018). In vivo impact testing on a lengthened femur with external fixation: A future option for the non-invasive monitoring of fracture healing? *Journal of The Royal Society Interface*, *15*(142). https://doi.org/10.1098/rsif.2018.0068

Melvin, J. W. (1993). Fracture mechanics of bone. *Journal of Biomechanical Engineering*, *115*(4B), 549–554. https://doi.org/10.1115/1.2895538

Memorial Sloan Kettering Cancer Center. (n.d.). *CT scan vs. MRI: What's the difference? And how do doctors choose which imaging method to use?* Retrieved April 9, 2025, from https://www.mskcc.org/news/ct-vs-mri-what-s-difference-and-how-do-doctors-choose-which-imaging-method-use

Nikiforidis, G., Bezerianos, A., Dimarogonas, A., & Sutherland, C. (1990). Monitoring of fracture healing by lateral and axial vibration analysis. *Journal of Biomechanics*, *23*(4), 323–330. https://doi.org/10.1016/0021-9290(90)90060-g

Omsland, T. K., Ahmed, L. A., Grønskag, A., Schei, B., Emaus, N., Langhammer, A., Joakimsen, R. M., Jørgensen, L., Søgaard, A. J., Gjesdal, C. G., & Meyer, H. E. (2011). More forearm fractures among urban than rural women: The NOREPOS study based on the Tromsø study and the HUNT study. *Journal of Bone and Mineral Research*, *26*(4), 850–856. https://doi.org/10.1002/jbmr.280

Pinzaru, V., Bujoreanu, C., & Barat, O. (2024). Structural damping analysis of a vehicle front hood: Experimental modal parameters extraction and simulation correlation. *Machines*, *12*(12), Article 862. https://doi.org/10.3390/machines12120862

Ritchie, R. O., Kinney, J. H., Kruzic, J. J., & Nalla, R. K. (2005). A fracture mechanics and mechanistic approach to the failure of cortical bone. *Fatigue & Fracture of Engineering Materials & Structures*, *28*(4), 345–371. https://doi.org/10.1111/j.1460-2695.2005.00878.x

SDynPy. (n.d.). *Modal tutorial 05 part A: Computing frequency response from time data — SDynPy 0.14.2 documentation*. Retrieved June 4, 2025, from https://sandialabs.github.io/sdynpy/modal_tutorials/Modal_05_Experimental_Modal_Analysis/Modal_05a_Computing_FRF_from_Time_Data.html

Siemens. (n.d.). *What is a frequency response function (FRF)?* Retrieved June 4, 2025, from https://community.sw.siemens.com/s/article/what-is-a-frequency-response-function-frf

Sim, S. G., Woo, Y. J., Kim, D. Y., Hwang, S. J., Hwang, K. T., Lee, C. H., & Yoon, G. H. (2021). Experimental study of the effect of the boundary conditions of fractured bone. *Journal of the Mechanical Behavior of Biomedical Materials*, *124*, Article 104801. https://doi.org/10.1016/j.jmbbm.2021.104801

Van der Perre, G., & Lowet, G. (1996). In vivo assessment of bone mechanical properties by vibration and ultrasonic wave propagation analysis. *Bone*, *18*(1), S29–S35. https://doi.org/10.1016/8756-3282(95)00377-0

Van der Perre, G., Van Audekercke, R., Martens, M., & Mulier, J. C. (1983). Identification of in-vivo vibration modes of human tibiae by modal analysis. *Journal of Biomechanical Engineering*, *105*(3), 244–248. https://doi.org/10.1115/1.3138412

Wang, M., Gao, X., Abdel-Wahab, A., Li, S., Zimmermann, E. A., Riedel, C., Busse, B., & Silberschmidt, V. V. (2015). Effect of micromorphology of cortical bone tissue on crack propagation under dynamic loading. *EPJ Web of Conferences*, *94*, Article 03005. https://doi.org/10.1051/epjconf/20159403005

Wu, A.-M., Bisignano, C., James, S. L., Abady, G. G., Abedi, A., Abu-Gharbieh, E., Alhassan, R. K., Alipour, V., Arabloo, J., Asaad, M., Asmare, W. N., Awedew, A. F., Banach, M., Banerjee, S. K., Bijani, A., Birhanu, T. T. M., Bolla, S. R., Cámera, L. A., Chang, J.-C., ... Vos, T. (2021). Global, regional, and national burden of bone fractures in 204 countries and territories, 1990–2019: A systematic analysis from the Global Burden of Disease Study 2019. *The Lancet Healthy Longevity*, *2*(9), e580–e592. https://doi.org/10.1016/S2666-7568(21)00172-0

Yoon, G. H., Woo, Y. J., Sim, S. G., Kim, D. Y., & Hwang, S. J. (2021). Investigation of bone fracture diagnosis system using transverse vibration response. *Proceedings of the Institution of Mechanical Engineers, Part H: Journal of Engineering in Medicine*, *235*(5), 597–611. https://doi.org/10.1177/0954411921997575

Zimmermann, E. A., Busse, B., & Ritchie, R. O. (2015). The fracture mechanics of human bone: Influence of disease and treatment. *BoneKEy Reports*, *4*. https://doi.org/10.1038/bonekey.2015.112